Article

High piezoelectric conversion properties of axial InGaN/GaN nanowires

N. Jegenyes1, M. Morassi1, P. Chrétien2, L. Travers1, L. Lu1, F. H. Julien1, M. Tchernycheva1, F. Houzé2, N. Gogneau,1,*

[1] Centre de Nanosciences et de Nanotechnologies - CNRS-UMR9001, Université Paris-Saclay, France
[2] Laboratoire de Génie Électrique et Électronique de Paris, UMR 8507 CNRS-Centrale-Supélec, Université Paris-Sud Université Paris-Saclay et UPMC-Sorbonne Université, France
* Correspondence: noelle.gogneau@c2n.upsaclay.fr; Tel.: +33 (0)1 69 63 61 75

Abstract: We demonstrate for the first time efficient mechanical to electrical energy conversion using InGaN/GaN nanowires (NWs). Using an atomic force microscope equipped with a modified Resiscope module, we analyse the piezoelectric energy generation of GaN NWs and demonstrate an important enhancement when integrating in their volume a thick In-rich InGaN insertion. The piezoelectric response of InGaN/GaN NWs can be tuned as a function of the InGaN insertion thickness and position in the NW volume. The energy harvesting is favoured by the presence of a PtSi/GaN Schottky diode which allows to efficiently collect the piezo-charges generated by InGaN/GaN NWs. Average output voltages up to 330 ± 70 mV and a maximum value of 470 mV per NW has been measured for nanostructures integrating 70 nm-thick InGaN insertion capped with a thin GaN top layer. This latter value establishes an increase of about 35% of the piezo-conversion capacity in comparison with binary p-doped GaN NWs. By considering these output signals, we estimate a maximum power density generated by one layer of dense InGaN/GaN-based NW of about 3.3 W/cm2. These results settle the new state-of-the-art for piezo-generation from GaN-based NWs and offer a promising perspective for extending the performances of the piezoelectric sources.

Keywords: III-N Nanowires; Piezoelectric generation; Atomic force microscope; Piezo-generators; Energy harvesting

1. Introduction

The number of nomad micro-devices for medical implants, sensing, monitoring and personal electronics is constantly rising in our daily life, and the development of autonomous power supply systems constitutes an important challenge. Today, the most common solution for self-supplying micro-systems consists in using batteries. Despite the recent progress in the development of batteries with high energy density [1-2], these sources present limitations such as their complex integration, their limited capacity and their cost. In this context, the development of new energy generation technologies relying on ultra-compact and integratable sources and generating sufficient power to supply the micro-devices without increasing their weight is vital for sustainable, independent and maintenance-free operation of micro-devices.

Small-scale energy harvesting, i.e. the conversion of ambient energy into the supply energy required for an embedded system, is a promising perspective, as it would make the micro-devices energy-autonomous, without the need of grid connection or batteries. Among the alternative ambient energy resources, the mechanical vibrations and deformations, that can be harvested using piezoelectric materials, present the advantages in many environments to be ubiquitous available at all time and more accessible than solar and thermal energy. These energies may have various origins, such as body movements, sound vibrations, hydraulic movements, wind, friction...

In the last decade, thanks to the break-through in the synthesis of nanomaterials, 1D piezoelectric nanostructures (such as nanowires (NWs), nanorods, nanofibers…) have emerged as

excellent candidates to fabricate novel ultra-compact and highly efficient piezo-generators, then opening new application fields, such as the powering of wireless micro-devices. Their attractiveness stems from their superior mechanical properties [3-4], higher sensitivity to applied force [4-5] and higher piezoelectric coefficients [6-8] in comparison to conventional 2D films and bulk materials.

Since the first demonstration of electrical generation from the lateral bending of ZnO NWs in 2006, then defining for the first time the nanogenerator concept [9], other 1D-nanostructures have been investigated such as NWs of CdS [10], CdSe [11], PZT [12], BaTiO3 [13], KNBO3 [14] … These last years, the attention has turned to III-nitride NWs thanks to their high-piezoelectric coefficients [15] and their strong piezo-generation response. The first mechanical-electrical conversion from GaN nanorods has been reported in 2007 [16]. But it is only starting from 2010, that III-nitride 1D-nanostructures are investigated as potential nanomaterials for piezoelectric generation. To date, the best mechanical-electrical conversion from NWs in terms of the output voltage has been obtained with n-doped GaN and InN NWs, with a maximum generated voltage per NW of about -440 mV [17] and 1 V [18], respectively. These outputs illustrate the high potential of nitride 1D-nanostructures for developing efficient piezo-generators, since they largely exceed those for other piezoelectric nanostructures and especially ZnO NWs which are today the most studied nanomaterials for piezo-conversion.

The studies of the piezoelectric properties of individual 1D-nanostructures have naturally lead to the fabrication of macroscopic piezo-generators with different designs and integrating various 1D-nanostructures such as PVDF nano-materials [19-21], PZT nanofibers [22], ZnO [23-24] or III-nitride NWs [25-27]. While these energy sources can generate power densities in the μW-mW/cm3 range, their use as micro-system power supplies is rather limited, especially due to their poor energy conversion. Indeed, to reach these generation capacities, devices of several square centimetres in size, and /or the application of pressures of the order of several MPa are required, not allowing their use as viable integrated energy sources. To consider the NW-based energy harvesting systems for supplying micro-devices, the improvement of the conversion capacity and efficiency of the piezoelectric active layer is a pre-requisite to the extension of the generator performances.

In this work, we demonstrate that the energy generation capacity and efficiency of GaN nanowires can be enhanced by integrating an In-rich InGaN section in the NW volume. Using an atomic force microscope equipped with a modified Resiscope module [17], we systematically investigate the piezo-conversion properties of individual MBE-grown p-doped In0.35GaN0.65/GaN NWs in a dense array. We establish that the piezoelectric response of InGaN/GaN heterostructure NWs can be tuned as a function of the InGaN insertion thickness and its position in the NW volume. We also evidence that the energy harvesting is more efficient when InGaN insertion is capped with a thin GaN layer since the PtSi/GaN Schottky nano-contact, through which are collected the generated piezo-charges, leads to an improved conductance in comparison with PtSi/InGaN Schottky one. Hence, we report average output voltages up to ◎ 330 ± 70 mV and a maximum value of 470 mV per NW integrating 70 nm-thick InGaN insertion capped with a thin GaN top layer. This result constitutes the first demonstration of mechanical-electrical conversion from axial InGaN/GaN NWs and highlight an enhancement of about 35% of the piezo-conversion capacity in comparison with non-heterostructured binary p-doped GaN NWs (maximum output voltage of 350 mV per NW [28]). By considering the maximum output signals, we have estimated a maximum output power of 223 pW per NW and a power density generated by one layer of InGaN/GaN NWs of about 3.3 W/cm2. These maximum powering capacities estimated from AFM measurements on free-standing NWs demonstrate the impact of InGaN insertion to enhance the energy generation and thus offer a promising perspective for the exploitation of InGaN/GaN heterostructured NWs as active media for high-efficient ultra-compact piezo-generators.

Peer-reviewed version available at Nanomaterials 2018, 8, 367; doi:10.3390/nano8060367

2. Materials and Methods

Self-assembled InGaN/GaN NWs were grown on conductive oxide-free Si(111) substrates (resistivity of the order of 0.007 Ω cm) in a molecular beam epitaxy chamber, equipped with a radio-frequency N plasma source. Prior to the growth of InGaN/GaN NWs, a 2.5-nm-thick AlN buffer layer was deposited on the substrate following a previously reported procedure [29], to allow for a better control of the NW nucleation, density and orientation [30-32]. The GaN NW bases were grown at 790 °C under N-rich conditions with an N/Ga flux ratio of 1.36 (Fig. 1a). Then, the substrate temperature was ramped down to 590°C under growth interruption to grow disk-shaped axial InxGa1-xN heterostructures with an average In content of x = 0.35 ± 0.05 (Fig. 1b) within the In-adlayer growth regime [33]. Following these growth conditions, we obtained highly homogeneous In-rich InxGa1-xN insertions as illustrated by the high angle annular dark field scanning transmission electron microscopy (HAADF-STEM) and EDX mappings of Figure 1c. In addition, in some samples, a GaN cap was grown on top under N-rich conditions (N/Ga ratio of 25) at 650°C to preserve abrupt InGaN/GaN interfaces.

The resulting InGaN/GaN NWs are vertically aligned with hexagonal cross-section shape delimited by {10-10} planes [34]. The NWs are also characterized by N-polar top surface (NWs grown along the [000-1] direction), which implies that under compressive strain the resulting piezoelectric potential created inside the nanostructures is positive, while under tensile strain the potential is negative as explaining in details in ref. [35].

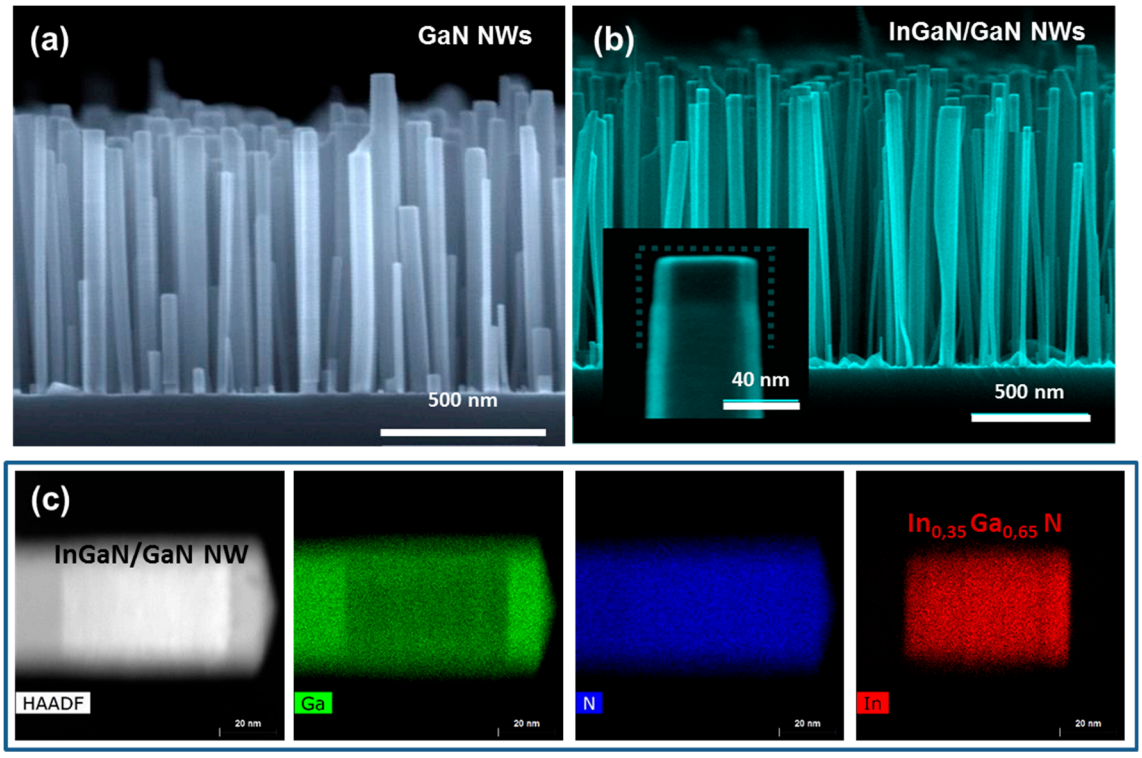

Figure 1. Scanning electron microscope images of (a) GaN and (b) InGaN/GaN NWs grown by plasma-assisted MBE. (c) Transmission electron microscope image and Ga, N and In EDX mappings of the top part of a capped InGaN/GaN NW.

In the present work, three different sets of samples were investigated, as schematize on Fig. 2a. Two sets consisted of InGaN/GaN NWs with a single uncapped InGaN insertion (of 35 ± 5 nm and 70 ± 10 nm thickness respectively) localized on the GaN NW top (SEM micrograph of Fig. 1b); while the third set had a 70 ± 10 nm thick InGaN section capped with a 10 nm-thick GaN layer (Fig. 1c). For each series, the NWs are characterized by a length of 1.1 ± 0.1 μm, a diameter of 50 ± 20 nm and a density of the order of 1.5x1010 NW/cm2.

Peer-reviewed version available at Nanomaterials 2018, 8, 367; doi:10.3390/nano8060367

In order to measure accurately the piezoelectric response of individual NWs (with the AFM system described below), and because the III-N NWs are characterized by a high flexibility, the NWs have been mechanically consolidated by embedding their bottom portion in an 850 nm thick polydimethylsiloxane (PDMS) layer (Fig. 2a). This flexible matrix allows ensuring the mechanical consolidation of the NWs without applying to them any deformation or strain (as verified by Raman spectroscopy measurements non-presented here). The height of the emerging NW portions is of about 250 ± 100 nm, while the density of the NWs remains unchanged.

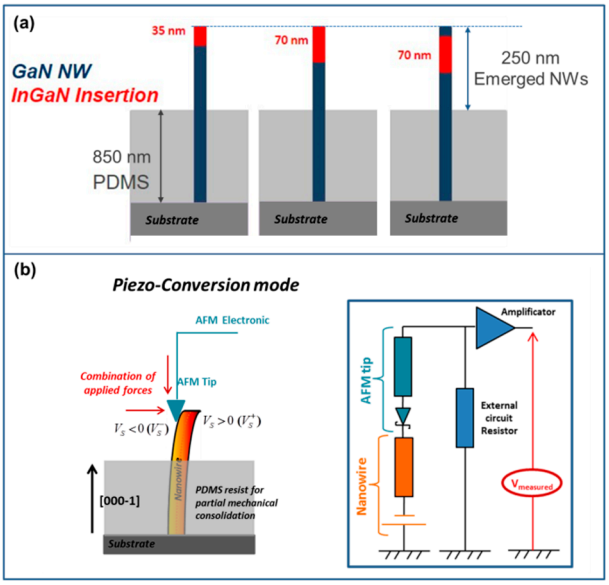

Figure 2. a) Schematization of the investigated structures: GaN NW base with an InGaN insertion localized on the top. From left to right: 35 ± 5 nm uncapped InGaN section and 70 ± 9 nm uncapped and capped InGaN insertions. (b) Schematic representation of the piezo-generation measurement principle on single NWs, using an AFM system in vertical configuration equipped with a modified Resiscope module. To perform accurate piezo-conversion measurements under AFM, the NWs have been mechanically consolidated with a 850 nm thick PDMS matrix, the emerged NW height being of the order of 250 nm.

The piezoelectric conversion properties of the NWs have been investigated by using an atomic force microscope in the vertical configuration equipped with a modified Resiscope module [17]. This method combines the nanometric scale resolution of the AFM and the real-time electrical measurement of the Resiscope [36] allowing resistance measurements over a ten decades range (102–1012 ⍵) in the dynamic conditions of AFM imaging. In this experimental configuration, the AFM tip scans over the surface of the NWs array in contact mode and under a controlled and constant normal force. The AFM tip induces a lateral deflection of the nanostructure, which results in the appearance of an asymmetric strain across the NW, from a tensile strain to the outer face of the NW to a compressive one to the inner face. As a consequence, a piezoelectric field is created inside the NW evolving respectively from negative to positive value [35] as schematized in Fig. 2b. The electrical response of the NW is monitored by the modified Resiscope. This electrical module is connected to the substrate and to a conductive AFM tip. An ohmic contact is formed between the NWs bottom and the substrate [37]. Conversely, between the NW top and the AFM tip, because we use a PtSi tip characterized by a work function of about 5 eV [38] and because the electron affinity of the GaN is 4.1 eV, the PtSi–GaN contact forms a Schottky barrier that ensures the charge recuperation for piezo-generation [39]. Throughout the measurements, both the topographic and the electrical signals are recorded simultaneously. In our specific instrumental configuration, we do not apply any external voltage and the voltage waveform generated by the NW is observed across a load resistance RL of 1 GΩ. This experimental technique allows characterizing the piezo-conversion properties of single NWs over a large surface, which provides statistic measurements.

3. Results

Figure 3 presents 3D mappings of output voltage peaks generated by the three sets of InGaN/GaN NW arrays recorded for constant normal force (CNF) of 100 and 200 nN. (Intermediate CNF values of 30, 60 and 150 nN were also tested but corresponding images are not presented for the sake of length). It must be mentioned that the CNF is much higher than the one (few nN) used for characterizing the free-standing ZnO [9] and other 1D-nanostructures by using equivalent AFM equipment. In fact, as detailed before, the NWs are mechanically consolidated due to their high flexibility. In consequence, a higher deflection force is needed to bend the emerging NWs and thus reach the same degree of deformation as the free-standing nanostructures. In the electrical mappings, each peak corresponds to the piezoelectric response of an individual NW and exhibits a positive output voltage. This is in agreement with the p-type conductivity of the NWs induced by using Magnesium during their growth [28, 40]. Results presented in Fig. 3 constitute the first demonstration of piezoelectric conversion from InGaN/GaN-based NWs.

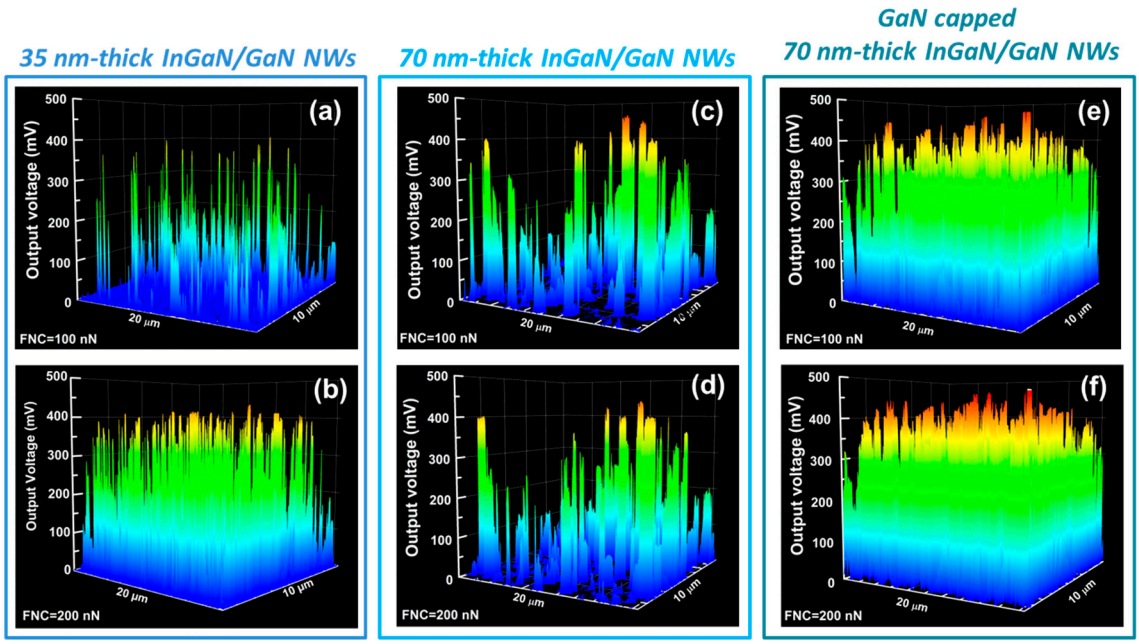

Figure 3. 3D output voltage mappings collected on (a-b) 35 nm-thick InGaN/GaN; (c-d) 70 nm-thick InGaN/GaN; and GaN capped 70 nm-thick InGaN/GaN NWs (e-f) using an AFM equipped with a modified Resiscope module in piezo-generation configuration for two different constant normal forces of 100 and 200 nN.

The maximum and average output voltages are presented in the Table 1 and in Figure 4 for each set of samples as a function of the CNF. The output voltages statistics showed a bimodal distribution, well approximated by two Gaussian functions. The error bars in Table 1 correspond to half-width at half maximum of the corresponding Gaussian fits.

The piezoelectric response of NWs strongly depends on their flexibility, which itself depends on the NW dimensions. In the present case, the height of the NWs emerging from the PDMS matrix is about 250 nm ± 100 nm (Fig. 2a). The small protruding NWs (height up to 150-200 nm) are characterized by a high rigidity which limits their deformation by bending and thus the creation of an efficient piezoelectric potential inside the nanostructure. By contrast, for higher NWs, the flexibility being more important, it is easier to reach a higher piezoelectric-field, then allowing the generation of a larger output voltage. In our experimental configuration, since each mapping has been probed with the same constant normal AFM tip force, during a scan, the output distribution reflects the flexibility dispersion of the NWs. We can thus attribute the double dispersion of measured output voltages (illustrated in Fig. 4b for two statistics) to the height dispersion of the NWs, which originates from the self-assembled growth mode used to synthesis them.

Preprints (www.preprints.org) | NOT PEER-REVIEWED | Posted: 30 April 2018 doi:10.20944/preprints201804.0383.v1

Peer-reviewed version available at Nanomaterials 2018, 8, 367; doi:10.3390/nano8060367

Table 1. Average values, standard deviations and maximal output voltages (with a measurement precision of 2%) generated by NWs as a function of the constant normal force.

Constant normal force (nN)	Average output voltage/ Standard deviation (mV) *Double distribution of the output voltages*			Maximum output voltage (mV)		
	35nm-InGaN	70 nm-InGaN	Capped 70 nm-InGaN	35nm-InGaN	70 nm-InGaN	Capped 70 nm-InGaN
30	*48 ± 29* *158 ± 93*	*46 ± 15* *199 ± 33*	*79 ± 60* *208 ± 87*	*340*	*411*	*446*
60	*66 ± 58* *198 ± 95*	*86 ± 80* *246 ± 45*	*96 ± 78* *257 ± 82*	*357*	*452*	*470*
100	*49 ± 53* *232 ± 102*	*94 ± 25* *263 ± 86*	*152 ± 72* *310 ± 109*	*385*	*453*	*472*
150	*75 ± 62* *239 ± 92*	*93 ± 25* *273 ± 90*	*175 ± 71* *330 ± 96*	*406*	*454*	*470*
200	*84 ± 60* *253 ± 64*	*94 ± 43* *296 ± 61*	*182 ± 61* *333 ± 70*	*423*	*444*	*472*

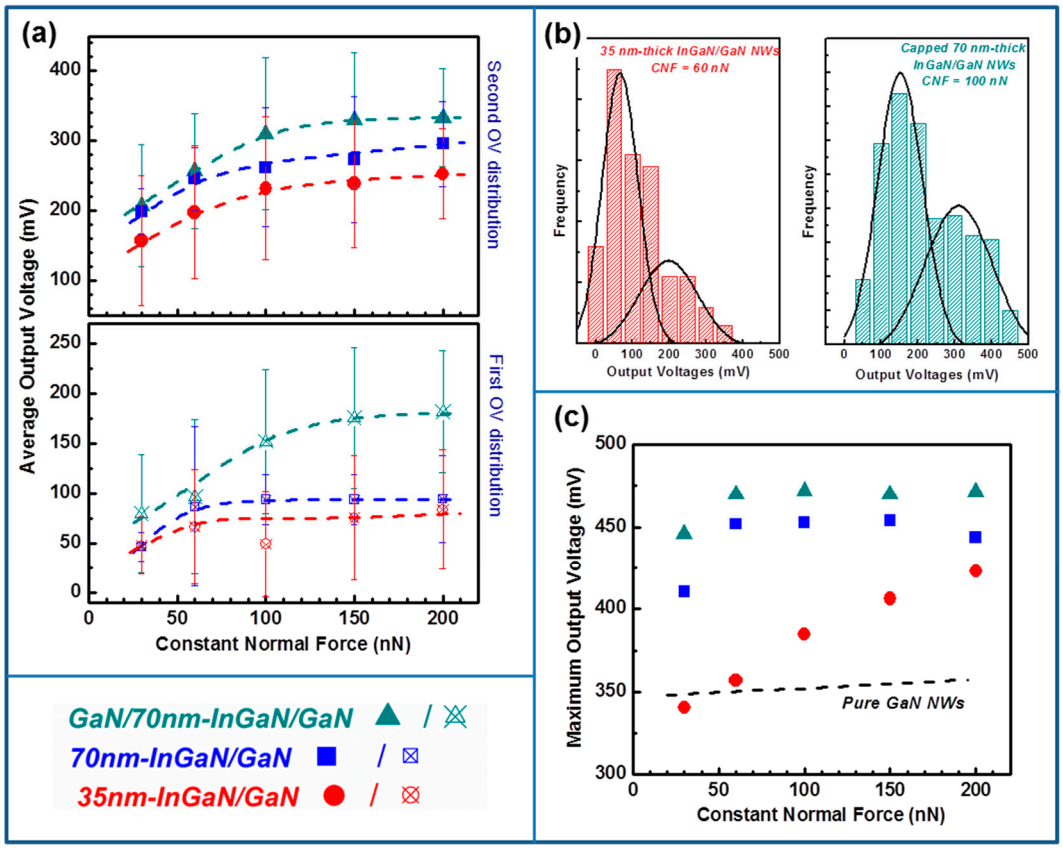

Figure 4. (a) Average and (c) maximum output voltages measured on InGaN/GaN NWs as a function of the constant normal force for the three sets of samples. For comparison, the maximum output voltages generated by non-heterostructured binary p-doped GaN NWs (from [28]) are also represented on (c). (b) Histogram distribution of the output voltages generated by 35 nm-thick uncapped InGaN/GaN and 70 nm-thick capped InGaN/GaN NWs respectively for CNF of 60 and 100 nN.

Peer-reviewed version available at Nanomaterials 2018, 8, 367; doi:10.3390/nano8060367

For the three sets of samples, we can clearly observe an increase of the output voltages with the constant normal force, in agreement with experimental results [17, 28, 41] and theoretical predictions [42]. This behaviour is explained by the convolution of two phenomena: (i) the increase of the piezoelectric potential with the increase of the NW deflection; (ii) and the improvement of the Schottky contact stability with increasing force applied by the conductive AFM tip [38, 43], and thus allowing a better harvesting efficiency.

Our results also evidence that the insertion of InGaN section in the volume of p-doped GaN NWs induces an improvement of piezoelectric response of the NWs in comparison with binary p-doped GaN NWs. This behaviour is well illustrated on Fig. 4c, where the maximum output voltages generated by the different sets of samples, as well as the measured ones for binary p-doped GaN NWs [28], have been plotted as a function of the constant normal force. The observed saturation of the generated outputs can be explained by a saturation of the internal electric field inside the NWs, resulting from the saturated rotation of electric dipoles [44], and/or by a limitation of the harvested energy through the Schottky contact, as we have recently reported [38].

For the highest applied CNF (200 nN), the piezo-conversion measurements assessed by AFM yield average output voltages per NW in the 253-333 mV range and maximum ones in the 423-472 mV range. These latest values largely exceed the maximum voltages generated by other families of piezoelectric 1D-nanostructures (PZT, CdS, CdSe …) and especially ZnO NWs (max. 90 mV per NW [45]), the widely investigated nanostructures for developing piezo-generators. Especially, for GaN-capped 70 nm-thick InGaN/GaN NWs, the maximum output reaches 470 mV per NW, then demonstrating an improvement of approximately 35 % of their piezo-conversion capacity in comparison with p-doped GaN NWs [28, 38], as well as an improvement by 7 % in comparison with the highest reported voltage for single n-doped GaN NWs [17]. This result settles thus the new state-of-the-art for piezoelectric generation from GaN-based NWs and demonstrates the high potential of InGaN/GaN NWs for developing efficient generators.

The integration of one InGaN insertion in the GaN NW volume results unambiguously in an improvement of its generation capacity. At this stage, one may wonder which mechanism is in play. The InGaN material is characterized by higher piezoelectric coefficients in comparison with GaN [46]. An equivalent degree of deformation will thus induce the appearance of a more important piezoelectric field inside the NW containing InGaN, and thus the generation of a higher output voltage. This behaviour is confirmed if we analyse the results from the point of view of the InGaN insertion thickness (35 nm-thick and 70 nm-thick InGaN/GaN NWs). In fact, as the insertion thickness increases, the piezo-generated output voltages also increase (Fig. 4). The InGaN insertion is integrated at the NW top, where the deformation is more pronounced. The increase of the piezo-generated energy is thus more important when the InGaN insertion is thick and thus the locally created piezoelectric field is higher. This behaviour is experimentally confirmed by the different conversion efficiencies observed in Fig. 4 between the uncapped 35 nm-thick and 70 nm-thick InGaN/GaN NWs. For thinner insertion, the maximum output voltages increase quasi-linearly with applied force, while for the thicker one, the outputs saturate for constant normal force larger than 60 nN. This evolution of the generated signals illustrates lower conversion efficiency in the case of the 35 nm-thick insertions which results from the creation of a smaller piezoelectric field in comparison with the thicker insertion, for an equivalent deformation force. Fig. 5 schematizes this mechanism by illustrating the piezoelectric field distribution and the corresponding output voltages for binary GaN, and uncapped 35 nm-thick InGaN/GaN and 70 nm-thick InGaN/GaN NWs.

Preprints (www.preprints.org) | NOT PEER-REVIEWED | Posted: 30 April 2018 doi:10.20944/preprints201804.0383.v1

Peer-reviewed version available at Nanomaterials 2018, 8, 367; doi:10.3390/nano8060367

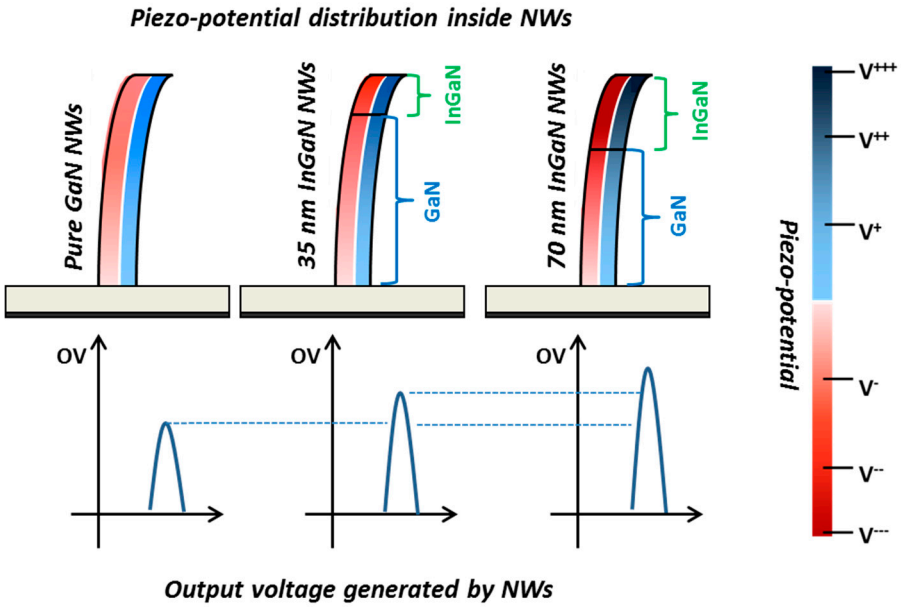

Figure 5. Schematization of the piezo-potential distribution as a function of the NW hetero-structuration and the corresponding output voltage generated for binary GaN NWs (left side), 35 nm-thick InGaN/GaN NWs (middle) and 70 nm-thick InGaN/GaN NWs (right side). The thicker is the InGaN insertion, the higher is the piezo-potential and the larger is the output voltage.

If now, we compare the piezo-generation of uncapped and GaN-capped 70 nm-thick InGaN/GaN NWs (Figs. 3 and 4), one may wonder why the presence of a GaN cap layer leads to an improvement of the piezo-response of the system. The measured output voltage depends mostly on the capacity of the piezoelectric material (here the NWs) to efficiently convert the mechanical deformation into electrical energy. However, it also strongly depends on the efficiency of the metal/semiconductor electrode to harvest the piezo-generated energy. By capping with GaN the 70 nm-thick InGaN insertion, we have modified the characteristics of the Schottky diode formed between the PtSi AFM tip and the NW. We have recently demonstrated that because the AFM tip/NW contact is governed by its nanometer size, the conventional description of the Schottky diode cannot be applied [38]. In the case of Schottky nano-contact, the effective Schottky barrier height becomes a function of the diode size. In this condition, the contribution of the tunnelling emission becomes dominant and thus gives rise to an improved energy harvesting [47-48].

The diode size is directly related to the AFM tip radius (which is of 25 nm for PtSi AFM tip [38]) and to the properties of the material constituting the top surface of the NW. We have calculated the contact surface between the PtSi AFM tip and the InGaN, GaN and InN NW top by using the Hertz theory [38, 49]. This theory describes a regime of purely elastic deformation between two perfectly smooth solids, in the absence of adhesion and friction. In these conditions, the mechanical contact between a sphere of radius R (here the AFM tip radius) and a plane (here the GaN top NW surface) is expressed as a disk of radius a by the following equation: $a = \left(\frac{3}{4}\frac{F\,R}{E^*}\right)^{1/3}$, where F is the applied force, R is the AFM tip radius and E* is the reduced Young's modulus of the two materials and given by $\frac{1}{E^*} = \left(\frac{1-\nu_1^2}{E_1}\right) + \left(\frac{1-\nu_2^2}{E_2}\right)$ with E1, E2 and ◎1, ◎2 are respectively the Young's modulus and Poisson's ratios of the two materials. The materials parameters considered for the calculations are presented in the Table 2. The InGaN parameters have been calculated by considering the Vegard's Law with the elastic parameters of bulk GaN and InN [50], and an In content of 35 %. To illustrate our approximation of the InGaN parameters, we have represented on figure 6 the contact radius for PtSi/InN interface.

Table 2. Material settings used for the calculations (* refer to bulk values).

	GaN	InGaN	InN	PtSi
Young's modulus *E* (GPa)	**300*** [51]	**244**	**149*** [53]	**238** [55]
Poisson coefficient *ν*	**0.4** [52]	**0.25**	**0.365** [54]	**0.32** [55]

Fig. 6 presents the calculated contact radius for both uncapped and GaN-capped InGaN/GaN NWs as a function of the constant normal force. We can observe that whatever the Schottky diode, the contact radius, which is extremely small (of about few nm), is lower than the depletion width in III-N NW, which typically varies between 20 and 80 nm depending on the dopant density and/or the NW diameter [56-58]. This result confirms the nano-contact behaviour of the Schottky diode. Then, the smaller is the diode size, the thinner is the barrier and the higher is the conductance. Because at a given force the contact radius is smaller for the GaN/PtSi interface than for the InGaN/PtSi one, the harvested energy is increased. This result is consistent with the increased output voltages measured for the capped NWs under nominally identical CNF.

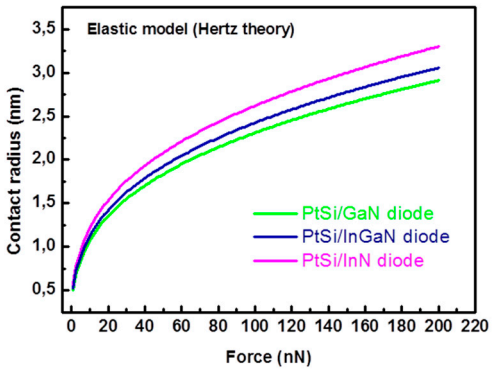

Figure 6. Calculation of the contact radius between PtSi AFM tip and GaN (green line), InN (pink line) and InGaN (blue line) NWs as a function of the applied force. The Hertz theory has been used with the material setting from Table 2.

The experimental results presented in this work demonstrate that the piezoelectric conversion of GaN NWs is substantially enhanced by the presence of axial InGaN heterostructures. Hence, the integration of these nanostructures appears as a promising solution for improving the piezoelectric generator performances. In order to illustrate this high potential, we have estimated the capacity of the three sets of NW samples for powering nano-devices. To determine the maximal output power density generated by our p-doped InGaN/GaN NWs, we have considered the following relation: $P = \frac{\overline{V_i^2}}{R_L} \cdot \rho$, where V_i is the output voltage generated by the i-th NW, R_L is the resistance across which the measurement is performed ($R_L = 1\,G\Omega$) and ρ is the surface density of NWs. Assuming that each NW produces the maximal output voltage for a constant normal force of 200 nN, and that the NW density was about 1.5x1010 NW/cm2, we have estimated and reported in Table 3 the maximum output power and the maximum power densities for the three sets of samples. The estimated values are, respectively, in the 179-223 pW per NW and in the 2.7 – 3.3 W/cm2 ranges. These values, to the best of our knowledge, exceed all previously reported ones assessed by AFM technique. Regarding the high powering capacity of these free-standing, the InGaN/GaN-based NWs present high potentialities for developing integratable and high-efficient piezoelectric energy harvested sources.

Table 3. Maximum output voltages, output powers and power densities of 35 nm-thick InGaN/GaN; 70 nm-thick InGaN/GaN; and GaN capped 70 nm-thick InGaN/GaN NWs at a constant normal force of 200 nN.

Constant normal force (nN)	Maximum output voltage (mV)			Maximum output power (pW per NW)			Maximum power density (W/cm²)		
	35nm-InGaN	70 nm-InGaN	Capped 70 nm-InGaN	35nm-InGaN	70 nm-InGaN	Capped 70 nm-InGaN	35nm-InGaN	70 nm-InGaN	Capped 70 nm-InGaN
200	*423*	*444*	*472*	*179*	*197*	*223*	*2.7*	*3*	*3.3*

5. Conclusions

In summary, we have demonstrated for the first time the high piezoelectric response of InGaN/GaN-based NWs. Using an AFM equipped with a modified Resiscope module, we have shown that it is possible to tune the piezo-conversion properties of individual MBE-grown p-doped In0.35GaN0.65/GaN NWs by modulating the InGaN insertion thickness and position in the NW volume. Based on piezo-response assessed by AFM and on calculation of the Schottky diode size using the Hertz theory, we have evidenced that the conductance at the PtSi/GaN Schottky nano-contact is more favourable in comparison to the PtSi/InGaN one, and thus yields an improvement of the piezoelectric harvesting. Hence, under lateral deformation of the NWs, an average output voltage up to ◎ 330 ± 70 mV and a maximum value of 470 mV per NW integrating a 70 nm-thick InGaN insertion capped with a thin GaN top layer have been reported. This latter value is larger by 35 % in comparison with p-doped GaN NWs (maximum output voltage of 350 mV per NW [28]), and larger by 7 % in comparison with the highest reported voltage for single n-doped GaN NWs (maximum output voltage of -442 mV per NW [17]). This result settles thus the new state-of-the-art for piezoelectric generation from GaN-based NWs and demonstrates the high potential of InGaN/GaN NWs for developing efficient generators. By considering the maximum output signals measured by AFM on free-standing NWs, we have estimated a maximum output power of 223 pW per NW and a power density generated by one dense layer of InGaN/GaN NWs of about 3.3 W/cm2. These results demonstrate the capability of InGaN insertion to enhance the energy generation and thus offering a promising perspective to develop ultracompact and integrable renewable energy sources for sustainable, independent and maintenance-free operation of microdevices.

Author Contributions: For research articles with several authors, a short paragraph specifying their individual contributions must be provided. The following statements should be used "Conceptualization, X.X. and Y.Y.; Methodology, X.X.; Software, X.X.; Validation, X.X., Y.Y. and Z.Z.; Formal Analysis, X.X.; Investigation, X.X.; Resources, X.X.; Data Curation, X.X.; Writing-Original Draft Preparation, X.X.; Writing-Review & Editing, X.X.; Visualization, X.X.; Supervision, X.X.; Project Administration, X.X.; Funding Acquisition, Y.Y.", please turn to the CRediT taxonomy for the term explanation. Authorship must be limited to those who have contributed substantially to the work reported.

Funding: This work was financially supported by the by EU Horizon 2020 ERC project 'NanoHarvest' (Grant 639052), the French National Research Agency through the GANEX program (ANR-11-LABX-0014) and the Region Ile-de-France in the framework of DIM Nano-K.

Acknowledgments: In this section you can acknowledge any support given which is not covered by the author contribution or funding sections. This may include administrative and technical support, or donations in kind (e.g. materials used for experiments).

Conflicts of Interest: Declare conflicts of interest or state "The authors declare no conflict of interest." Authors must identify and declare any personal circumstances or interest that may be perceived as inappropriately influencing the representation or interpretation of reported research results. Any role of the funding sponsors

in the design of the study; in the collection, analyses or interpretation of data; in the writing of the manuscript, or in the decision to publish the results must be declared in this section. If there is no role, please state "The founding sponsors had no role in the design of the study; in the collection, analyses, or interpretation of data; in the writing of the manuscript, and in the decision to publish the results".

References

1. Armand, M.; Endres, F.; MacFarlane, D. R.; Ohno, H.; Scrosati, B. Ionic-liquid materials for the electrochemical challenges of the future. *Nat Mater.* **2009**, 8, 621
2. Miller, J. R.; Simon, P. Electrochemical Capacitors for Energy Management. *Science* **2008**, 321, 651
3. Wen, B.; Sader, J. E.; Boland, J. J.; Mechanical Properties of ZnO Nanowires. *Phys. Rev. Lett.* **2008**, 101, 175502
4. Wang, X. Piezoelectric nanogenerators—Harvesting ambient mechanical energy at the nanometer scale. *Nano Energy* **2012**,1, 13
5. Zhou, Y. S.; Hinchet, R.; Yang, Y.; Ardila, G.; Sangmuang, R.; Zhang, F.; Zhang, Y.; Han, W.; Pradel, K.; Montès, L.; Mouis, M.; Wang, Z. L. Nano-Newton Transverse Force Sensor Using a Vertical GaN Nanowire based on the Piezotronic Effect. *Adv. Mater.* **2013**, 25, 883
6. Minary-Jolandan, M.; Bernal, R. A.; Kuljanishvili, I.; Parpoil, V.; Espinosa, H. D. Individual GaN Nanowires Exhibit Strong Piezoelectricity in 3D. *Nano Lett.* **2012**, 12, 970
7. Zhao, M. H.; Wang, Z. L.; Mao, S. X. Piezoelectric Characterization of Individual Zinc Oxide Nanobelt Probed by Piezoresponse Force Microscope. *Nano Lett.* **2004**, 4, 587
8. Agrawal, R.; Espinosa, H. D. Giant piezoelectric size effects in zinc oxide and gallium nitride nanowires. A first principles investigation. *Nano Lett.* **2011**, 11, 786
9. Wang, Z. L. Piezoelectric nanogenerators based on zinc oxide nanowire arrays. *Science* **2006**, 312, 242
10. Lin, Y. F.; Song, J.; Ding, Y.; Lu, S. Y.; Wang, Z. L. Piezoelectric nanogenerator using CdS nanowires. *Appl. Phys. Lett.* **2008**, 92, 022105
11. Zhou, Y. S.; Han, W.; Rai, S. C.; Zhang, Y.; Ding, Y.; Pan, C.; Zhang, F.; Zhou, W.; Wang, Z. L. Vertically Aligned CdSe Nanowire Arrays for Energy Harvesting and Piezotronic Devices. *ACS Nano* **2012**, 6, 6478
12. Chen, C. Y.; Liu, T H.; Zhou, Y.; Zhang, Y.; Chueh, Y. L.; Chu, Y. H.; He, Jr H.; Wang, Z. L. Electricity generation based on vertically aligned PbZr0.2Ti0.8O3 nanowire arrays. *Nano Energy* **2012**, 1, 424
13. Wang, Z.; Hu, J.; Suryavanshi, A. P.; Yum, K.; Yu, M. F. Voltage Generation from Individual BaTiO3 Nanowires under Periodic Tensile Mechanical Load. *Nano Lett.* **2010**, 10, 2966
14. Kang, P. G.; Lee, T. K.; Ahn, C. W.; Kim, I. W.; Lee, H. H.; Choi, S. B.; Jung, J. H. Vertically aligned epitaxial KNbO3 nanorod array for piezoelectric energy harvester and second harmonic generator. *Nano Energy* **2015**, 17, 261
15. Bernardini, F.; Fiorentini, V.; Vanderbilt, D. Spontaneous polarization and piezoelectric constants of III-V nitrides. *Phys. Rev. B* **1997**, 56, R10024(R)
16. Su, W. S.; Chen, Y. F.; Hsiao, C. L.; Tu, L. W. Generation of electricity in GaN nanorods induced by piezoelectric effect. *Appl. Phys. Lett.* **2007**, 90, 063110
17. Gogneau, N.; Chrétien, P.; Galopin, E.; Guilet, S.; Travers, L.; Harmand, J. C. ; Houzé, F. GaN nanowires for piezoelectric generators. Phys. Status Solidi RRL **2014**, 8, 414
18. Huang, C. T.; Song, J.; Tsai, C. H.; Lee, W. F.; Lien, D. H.; Gao, Z.; Hao, Y.; Chen, L. J.; Wang, Z. L. Single-InN-Nanowire Nanogenerator with Upto 1 V Output Voltage. *Adv. Mater.* **2010**, 22, 4008
19. Chang, C.; Tran, V. H.; Wang, J.; Fuh, Y. K.; Lin, L. Direct-write piezoelectric polymeric nanogenerator with high energy conversion efficiency. *Nano Lett.* **2010**, 10, 726
20. Serairi, L. « Elaboration et conception des dispositifs de la récupération d'énergie à base de nanofils de ZnO et de microfibres de PVDF-TrFE ». Physique [physics]. Université Paris-Est, 2017. Français. <NNT : 2017PESC1189>
21. Duan, Y.; Ding, Y.; Bian, J.; Xu, Z.; Yin, Z.; Huang, Y. Ultra-Stretchable Piezoelectric Nanogenerators via Large-Scale Aligned Fractal Inspired Micro/Nanofibers. *Polymers* **2017**, 9, 714
22. Chen, X.; Xu, S.; Yao, N.; Shi, Y. 1.6 V Nanogenerator for Mechanical Energy Harvesting Using PZT Nanofibers. *Nano Lett.* **2010**, 10, 2133
23. Zhu, G. A.; Yang, R. S.; Wang, S. H.; Wang, Z. L. Flexible High-Output Nanogenerator Based on Lateral ZnO Nanowire Array. *Nano Lett.* **2010**, 10, 3151
24. Zhu, G.; Wang, A. C.; Liu, Y.; Zhou, Y.; Wang, Z. L. Functional Electrical Stimulation by Nanogenerator with 58 V Output Voltage. *Nano Lett.* **2012**, 12, 3086

25. Lin, L.; Lai, C. H.; Hu, Y.; Zhang, Y.; Wang, X.; Xu, C.; Snyder, R L.; Chen, L. J.; Wang, Z. L. High output nanogenerator based on assembly of GaN nanowires. *Nanotechnology* **2011**, 22, 475401
26. Liu, G.; Zhao, S.; Henderson, R. D. E.; Leonenko, Z.; Abdel-Raman, A.; Mi, Z.; Ban, D. Nanogenerators based on vertically aligned InN nanowires. *Nanoscale* **2016**, 8, 2097
27. Jamond, N.; Chrétien, P.; Houzé, F.; Travers, L.; Harmand, J. C.; Glas, F.; Lefeuvre, E.; Tchernycheva, M.; Gogneau, N. Piezo-generator integrating a vertical array of GaN nanowires. *Nanotechnology* **2016**, 27, 325403
28. Gogneau, N.; Jamond, N.; Chrétien, P.; Houzé, F.; Lefeuvre, E.; Tchernycheva, M. From single III-nitride nanowires to piezoelectric generators: New route for powering nomad electronics. *Semicond. Sci. Technol.* **2016**, 31, 103002
29. Largeau, L.; Galopin, E.; Gogneau, N.; Travers, L.; Glas, F.; Harmand, J-C. N-Polar GaN Nanowires Seeded by Al Droplets on Si(111). *Cryst. Growth Des.* **2012**, 12, 2724
30. Brubaker, M. D.; Levin, I.; Davydov, A.V.; Rourke, D. M.; Sanford, N. A.; Bright, V. M.; and Bertness, K. A. GaN based nanorods for solid state lighting. *J. Appl. Phys.* **2011**, 110, 053506
31. Songmuang, R.; Landré, O.; and Daudin, B. Molecular beam epitaxy growth and optical properties of AlN nanowires. *Appl. Phys. Lett.* **2007**, 91, 251902
32. Bertness, K. A.; Roshko, A.; Mansfield, L. M.; Harvey, T. E.; and Sanford, N. A. First International Symposium on Growth of Nitrides. *J. Cryst. Growth* **2007**, 300, 94
33. Morassi, M.; Largeau, L.; Oehler, F.; Song, H-G.; Travers, L.; Julien, F. H.; Harmand, J-C.; Cho, Y-H.; Glas, F.; Tchernycheva, M.; Gogneau, N. Morphology Tailoring and Growth Mechanism of Indium-Rich InGaN/GaN Axial Nanowire Heterostructures by Plasma-Assisted Molecular Beam Epitaxy. *Crystal Growth and Design* **2018**, 18, 2545.
34. Largeau, L.; Dheeraj, D.L.; Tchernycheva, M.; Cirlin, G.E.; Harmand, J-C. Facet and in-plane crystallographic orientations of GaN nanowires grown on Si(111). *Nanotechnology* **2008**, 19, 155704
35. Gogneau, N.; Chrétien, P.; Galopin, E.; Guilet, S.; Travers, L.; Harmand, J. C.; Houzé, F. Impact of the GaN nanowire polarity on energy harvesting. *Appl. Phys. Lett.* **2014**, 104, 213105
36. O. Schneegans, P. Chrétien, F. Houzé, Patents WO-2011138738A1 (2011) ; EP-2567245A1 (2013)
37. Jacopin, G.; De Luna Bugallo, A.; Rigutti, L.; Lavenus, P.; Julien, F. H.; Lin, Y. T.; Tu, L. W.; Tchernycheva, M. Interplay of the photovoltaic and photoconductive operation modes in visible-blind photodetectors based on axial p-i-n junction GaN nanowires. *Appl. Phys. Lett.* **2014**, 104, 023116
38. Jamond, N.; Chrétien, P.; Gatilova, L.; Galopin, E.; Travers, L.; Harmand, J-C.; Glas, F.; Houzé F.; Gogneau. N. *Nanoscale* **2017**, 9, 4610
39. Liu, J.; Fei, P.; Song, J.; Wang, X.; Lao, C.; Tummala, R.; Wang, Z.L. Carrier Density and Schottky Barrier on the Performance of DC Nanogenerator. *Nano Lett.* **2008**, 8, 328
40. Lin, S. S.; Song, J. H.; Lu, Y. F.; Wang, Z. L. Identifying individual n- and p-type ZnO nanowires by the output voltage sign of piezoelectric nanogenerator. *Nanotechnology* **2009**, 20, 365703
41. Xu, X.; Potié, A.; Songmuang, R.; Lee, J. W.; Bercu, B.; Baron, T.; Salem, B.L.; Montès, L. An improved AFM cross-sectional method for piezoelectric nanostructures properties investigation: application to GaN nanowires. *Nanotechnology* **2011**, 22, 105704
42. Gao, Y.; Wang, Z.L. Electrostatic Potential in a Bent Piezoelectric Nanowire. The Fundamental Theory of Nanogenerator and Nanopiezotronics. *Nano Lett.* **2007**, 7, 2499
43. Perea-Garcia, B.; Zuniga-Perez, J.; Munoz-Sanjose, V.; Colchero, J.; Palacios-Lidon, E. Formation and Rupture of Schottky Nanocontacts on ZnO Nanocolumns. *Nano Lett.* **2007**, 7, 1505
44. Donald, J. L.; Engineering Analysis of Smart Material Systems, Wiley-Interscience: New-York, 2007, 124
45. Lu, M. P.; Song, J.; Lu, M. Y.; Chen, M. T.; Gao, Y.; Chen, L. J.; Wang, Z. L. Piezoelectric Nanogenerator Using p-Type ZnO Nanowire Arrays. *Nano Lett.* **2009**, 9, 1223
46. Akeuchi, T. T.; Mano, H. A.; Kasaki, I. A. Theoretical Study of Orientation Dependence of Piezoelectric Effects in Wurtzite Strained GaInN/GaN Heterostructures and Quantum Wells. *Jpn. J. Appl. Phys.* **2000**, 39, 413
47. Smit, G. D. J.; Rogge, S.; Klapwijk, T. M. Scaling of nano-Schottky-diodes. *Appl. Phys. Lett.* **2002**, 81, 3852
48. Smit, G. D. J.; Rogge, S.; Klapwijk, T. M. Enhanced tunneling across nanometer-scale metal–semiconductor interfaces. *Appl. Phys. Lett.* **2002**, 80, 2568
49. Johnson, K.L.; Contact Mechanics, Cambridge University Press, Cambridge, 1989
50. from http://www.ioffe.ru/SVA/NSM/Semicond/ website.

51. Bernal, R.A.; Agrawal, R.; Peng, B.; Bertness, K.A.; Sanford, N.A.; Davydov, A.V.; Espinosa, H. D. Effect of Growth Orientation and Diameter on the Elasticity of GaN Nanowires. A Combined in Situ TEM and Atomistic Modeling Investigation. *Nano Lett.* **2011**, 11, 548
52. Glas, F.; Daudin, B. Stress-driven island growth on top of nanowires. *Phys. Rev. B* **2012**, 86, 174112
53. Lu, Y-S.; Hsieh, C-H.; Gwo, S.; Hou, M. T.; Yao, J-S.; Yeh, J. A. An investigation of the Young's modulus of single-crystalline wurtzite indium nitride using an atomic force microscopy based micromechanical bending test. *Appl. Phys. Lett.* **2012**, 101, 221906
54. Gil, B. Low-dimensional Nitride Semiconductors, Oxford University Press (2002)
55. Koca, H.; Deligözb, E.; Mamedovc, A.M.; Philos. Mag. A 2011, 91, 3093
56. Simpkins, B. S.; Mastro, M. A.; Eddy Jr., C. R.; Pehrsson, P. E. Surface depletion effects in semiconducting nanowires. *J. Appl. Phys.* **2008**, 103, 104313
57. Tchoulfian, P.; Donatini, F.; Levy, F.; Dussaigne, A.; Ferret, P.; Pernot, J. Direct Imaging of p–n Junction in Core–Shell GaN Wires. *Nano Lett.* **2014**, 14, 3491
58. Calarco, R.; Stoica, T.; Brandt, O.; Geelhaar, L. Surface-induced effects in GaN nanowires. *J. Mater. Res.* **2011**, 26, 2157